Comparison of [^{68}Ga]Ga-DOTA-FAPI-04 PET/CT with [^{18}F]FDG PET/CT for Nodule Characterization and Staging in NSCLC Patients

Xin Zhou
Peking University Cancer Hospital: Beijing Cancer Hospital
Shuailiang Wang
Peking University Cancer Hospital: Beijing Cancer Hospital
Xiaoxia Xu
Peking University Cancer Hospital: Beijing Cancer Hospital
Xiangxi Meng
Peking University Cancer Hospital: Beijing Cancer Hospital
Huiyuan Zhang
Peking University Cancer Hospital: Beijing Cancer Hospital
Annan Zhang
Peking University Cancer Hospital: Beijing Cancer Hospital
Yufei Song
Peking University Cancer Hospital: Beijing Cancer Hospital
Hua Zhu
Peking University Cancer Hospital: Beijing Cancer Hospital
Zhi Yang
Peking University Cancer Hospital: Beijing Cancer Hospital
Nan Li (rainbow6283@sina.com)
Peking University Cancer Hospital: Beijing Cancer Hospital https://orcid.org/0000-0001-8619-7550

Research Article

Keywords: [68Ga]Ga-DOTA-FAPI-04, [18F]FDG, PET/CT , NSCLC, Diagnosis

Posted Date: April 27th, 2021

DOI: https://doi.org/10.21203/rs.3.rs-455463/v1

Abstract

Purpose:

The aim of this study is to explore the nodule characterization and staging efficacy of [^{68}Ga]Ga-DOTA-FAPI-04 PET/CT in non-small cell lung cancer (NSCLC) patients and to compare with that of [^{18}F]FDG PET/CT lesion-by-lesion.

Methods:

Sixty-five patients with clinically diagnosed or suspected NSCLC were enrolled in this prospective study (ChiCTR2000038080). All patients received both [^{18}F]FDG and [^{68}Ga]Ga-DOTA-FAPI-04 PET/CT, and they were assigned into three groups by different research directions as nodule characterization, node (N) staging and metastatic (M) staging. Imaging characteristics in PET/CT of lung nodules and suspected metastatic lesions were obtained and analyzed.

Results:

In the nodule characterization group, [^{18}F]FDG and [^{68}Ga]Ga-DOTA-FAPI-04 SUVmax ≥ 2.5 was set as the predictor of NSCLC, and the diagnostic sensitivity of [^{68}Ga]Ga-DOTA-FAPI-04 was higher than [^{18}F]FDG (0.88 vs. 0.67). And for adenocarcinoma with partial-solid density, SUV_{max} of ^{68}Ga-DOTA-FAPI-04 was higher than [^{18}F]FDG with significant differences (4.8 ± 2.8 vs. 2.1 ± 1.1). In N staging group, lymph nodes SUV_{max} of [^{68}Ga]Ga-DOTA-FAPI-04 was lower than [^{18}F]FDG in nonmetastatic group (3.1 ± 1.3 vs. 6.1 ± 2.3) and higher than [^{18}F]FDG (10.7 ± 4.7 vs. 6.5 ± 3.3) in metastatic group. Set 6 and 1.1 as the cut-off value for [^{68}Ga]Ga-DOTA-FAPI-04 SUV_{max} and [^{68}Ga]Ga-DOTA-FAPI-04 SUV_{max}/FDG SUV_{max}, diagnostic accuracy of metastatic lymph nodes using each criterion and their combination was 95%, 93% and 97% respectively. In multi-metastatic NSCLC patients, [^{68}Ga]Ga-DOTA-FAPI-04 identified more lesions than [^{18}F]FDG (206 vs. 106 lesions) and the uptake value of [^{68}Ga]Ga-DOTA-FAPI-04 was higher too, but no patients' staging was changed.

Conclusion:

Compared with [^{18}F]FDG, [^{68}Ga]Ga-DOTA-FAPI-04 PET/CT imaging has higher sensitivity in primary and metastatic lesion detection of NSCLC patients, it also increases the specificity of metastatic lymph nodes diagnosis.

Introduction

Cancer is associated with fibroblasts at all stages of disease progression including oncogenesis, proliferation and metastasis. The fibroblasts playing the subtle role in the regularization of tumor microenvironment have been recognized as cancer-associated fibroblasts (CAFs)[1–3]. The presence of

CAFs is associated with various types of tumor entities, including the non-small cell lung cancer (NSCLC) [4], in which the CAFs are commonly identified by their marker, fibroblast activation protein (FAP) [4–8]. FAP is a type II membrane-bound glycoprotein with dipeptidyl peptidase and endopeptidase activity, and is considered as a promising target for cancer theranostics[6, 8].

FAP-targeting molecules were recently developed as imaging and therapeutic agents based on the FAP-specific inhibitor (FAPI)[9]. In previous studies, FAPI-04 showed the most favorable pharmacokinetics in vivo, and was selected for further characterization in different tumor entities[10, 11]. A recent study demonstrated that among 28 types of tumor including NSCLC, high-quality images have been obtained with [^{68}Ga]Ga-DOTA-FAPI-04 PET/CT[12], confirming the high tumor uptake. Several systemic researches of prevalent cancers including glioblastomas, malignancies within the lower gastrointestinal tract, hepatic malignancies and head and neck cancers revealed the value of [^{68}Ga]Ga-DOTA-FAPI-04 in diagnosis, differential diagnosis and imaging-guided interventions [13–15]. According to previous studies, for NSCLC patients, [^{68}Ga]Ga-DOTA-FAPI-04 PET/CT might obtain good lesion detection in brain with low cerebral uptake, which is regarded as limitation for [^{18}F]FDG PET/CT[12, 16]. However, the impact of [^{68}Ga]Ga-DOTA-FAPI-04 PET/CT on NSCLC has not been studied systemically. The aim of this study is to explore the efficacy of [^{68}Ga]Ga-DOTA-FAPI-04 PET/CT in nodule characterization and staging for NSCLC patients, and to compare with that of [^{18}F]FDG PET/CT.

Materials And Methods

General

This is a prospective study in suspected and diagnosed NSCLC patients with paired [^{18}F]FDG and [^{68}Ga]Ga-DOTA-FAPI-04 PET/CT imaging performed between March 2020 and September 2020 (Trial registration ID: ChiCTR2000038080). This study was approved by the Medical Ethics Committee of Peking University Cancer Hospital (2019KT95), written informed consents were obtained from all participants. Details regarding the production of [^{68}Ga]Ga-DOTA-FAPI-04 can be found in supplementary information. Typically, 20 μg of DOTA-FAPI-04 was radiolabeled in each batch, yielding [^{68}Ga]Ga-DOTA-FAPI-04 with radiochemical purity over than 99%.

Patients and diagnostic criteria

The inclusion and exclusion criteria of patients are shown in **Fig 1**. The inclusion criteria are: (1) clinical diagnosed or suspected NSCLC patients who have undergone [^{18}F]FDG PET/CT for diagnosis and staging; (2) receiving a [^{68}Ga]Ga-DOTA-FAPI-04 PET/CT scan within 7 days after the [18F]FDG PET/CT scan; (3) confirmation of the diagnosis and staging by pathological evidences or reliable follow-up examinations. Exclusion criteria: (1) severe liver or kidney dysfunction; (2) chemoradiotherapy or targeted therapy before PET/CT scans. And the enrolled patients were assigned into three groups by different research directions as nodule characterization, node (N) staging, and metastatic (M) staging.

Pathological results and follow-up imaging results are adopted as the gold standard for lung nodules and lymph nodes (LNs) diagnosis. Pathological results are acquired from resection or aspiration biopsy. Follow-up imaging diagnosis criteria are set as follows: inflammatory nodules diagnosis must have completely resolution in the next six-month follow-up CT scans[17]; for metastatic LNs diagnosis, significant responses (at least 30% decrease in long diameters) to anti-tumor therapy should be in follow-up CT scans[18]; non-metastatic LNs diagnosis is defined as LNs with no morphological changes while obvious responses of primary tumor (≥30% decrease of long diameter) exist to anti-tumor therapy.

Examination Procedures

Patients were intravenously injected with [^{68}Ga]Ga-DOTA-FAPI-04 (1.9-3.7 MBq/kg) and underwent a whole-body scan 40-60 min p.i.. Imaging was performed on a Biograph mCT Flow 64 PET/CT scanner (Siemens Healthcare). PET images acquired in 3-dimensional mode using FlowMotion (Siemens Healthcare) at a speed of 1.5 mm/s from the vertex to the upper thigh for each subject. PET images, attenuation corrected with low-dose CT images, were reconstructed using an ordered-subsets expectation maximization (OSEM) method with 200 × 200 matrix, 2 iterations, and 11 subsets. The size of the post-reconstruction Gaussian filter was 5 mm. A high-resolution breath-holding CT scan was performed for each patient (120 kV, 146 mAs). CT images reconstructed using SAFIRE algorithm with 512 × 512 matrix and the slice thickness was 3-5 mm.

Patients' general information such as heart rate, respiratory rate, body temperature and blood pressure were measured before injection, during the scanning period, and every 6 hours after PET/CT scans for two days. All patients received the [^{18}F]FDG PET/CT scan first, and followed by a [^{68}Ga]Ga-DOTA-FAPI-04 PET/CT scan. Acquisition and reconstruction parameters of both scans remained consistent.

Imaging Analysis

Siemens workstation (Syngo.via VB20, MM Oncology) was used for image postprocessing. Two experienced nuclear medicine physicians blinded to the prior findings reviewed all images independently and any discordant results were resolved by consensus.

Longest diameter, location and size of the solid component from high-resolution CT were recorded. Nodules morphology, including lobulated, spicules of margin, pleural indentation, vacuole sign and calcification were depicted as well. Classification of nodules are defined as follows. Ground glass opacity (GGN): homogeneous opacities viewed using the lung window which cannot be viewed in mediastinal window; part-solid nodules (PSN), consisted of GGNs with a solid component both in the lung and mediastinal window; solid nodules (SN), solid component without GGN[19]. According to former researches[20, 21], $SUV_{max} \geq 2.5$ was set as the criterion for NSCLC diagnosis in [^{18}F]FDG PET, and the cut-off value for [^{68}Ga]Ga-DOTA-FAPI-04 PET SUV_{max} was also set as 2.5 based on the consensus of the participating physicians.

LNs of diagnosed NSCLC patients characterized by short diameter ≥ 0.5 cm and SUV_{max} of [^{18}F]FDG higher than the blood pool were considered as suspected metastatic LNs. Short and long axis dimension, density and calcification status of LNs were also depicted based on CT images. SUV_{max} and SUV_{mean} of lung nodules, metastatic lesions and blood pool from both [^{18}F]FDG and [^{68}Ga]Ga-DOTA-FAPI-04 PET/CT were obtained by software (Syngo.via). All LNs were classified into high, intermediate and low risks according to the risk categories based on the relationship of LNs location and lung nodules, which was specified in supplemental information[22]. The density of LNs was identified as high, iso and low density, compared with mediastinal soft tissue. SUV_{max}≥2.5 was also set as the criteria for metastatic LNs diagnosis in [^{18}F]FDG[23]. For multiple metastasis patients, the highest metabolic lesion was identified for each metastatic organ.

Statistics

One-way ANOVA was conducted, as well as statistical tests including Wilcoxon signed-rank test, Mann-Whitney U test, and Chi-square test, with the IBM SPSS Statistics (version 24; IBM Corp.) software. Logistic regression (Forward LR) was used to analyze the influence of parameters on metastatic or non-metastatic LNs. *P*-values of less than 0.05 were considered statistically significant.

Results

Patient Characteristics

Sixty-five patients were enrolled in this study in total, including 34 males and 31 females. The median age was 62 (32–79), and 34 patients had smoking history. Twenty-one patients had negative results of all lung tumor markers (NSE, CA199, CA125, SCC, CEA and CYFRA21-1) while 12 patients had single marker positive, and 14 patients with two or more markers positive. Number of patients in the three research groups are: nodules characterization (63 cases), N staging (35 cases) and M staging (9 cases) (Fig. 1).

Nodule characterization comparison of [^{68} Ga]Ga-DOTA-FAPI-04 and [^{18} F]FDG PET/CT in lung nodules

Sixty-eight lesions of 63 patients (two patients with three nodules and one patient with two nodules) were enrolled in the nodule characterization group. In reference to diagnosis, except for two inflammatory nodules diagnosed by follow-up CT imaging, pathological results of the other 66 lung nodules were obtained from either resection or aspiration biopsy. To analyze the tumor heterogeneity, 68 lung nodules were characterized as three types according to their pathological results: adenocarcinoma (AC, 51 lesions), squamous cell carcinoma (SCC, 9 lesions) and inflammation & granuloma (Inf & G, 8 lesions). Furthermore, all 68 lesions were also categorized by their density on CT images: 46 SN, 4 GGN and 18 PSN. Imaging characteristics and one-way ANOVA among groups are shown in Table 1. The density of SCC and Inf & G nodules were basically recognized as SN, while the density of AC nodules was different. Meanwhile, adenocarcinoma tended to have vacuoles, pleural indentation signs and lower uptake. Only

lobular sign incidence exhibited differences between NSCLC and Inf & G, but the other imaging characteristics did not.

Table 1
Imaging characteristics of lung nodules

Characteristics	AC (%)	SCC (%)	Inf & G (%)	*F*	*P*
Lesions	51	9	8		
Density					
SN	30 (58.8)	9 (100)	7 (87.5)		
PSN	17 (33.3)	0	1(12.5)	3.666	0.031#
GGN	4 (7.8)	0	0		
Long diameter(cm)	2.39 ± 1.17	2.47 ± 1.46	2.3 ± 0.73	0.038	0.963
Lobular sign	41 (80.4)	5 (55.6)	1 (12.5)	9.859	0.000*
Spiculation	45 (88.2)	7 (77.8)	7 (87.5)	0.354	0.703
Vacuole	28 (54.9)	1 (11.1)	2 (25)	4.007	0.023#
Pleural indentation	41 (80.4)	4 (44.4)	4 (50)	3.790	0.028#
Calcification	1 (2)	3 (33.3)	0	0.163	0.850
FDG SUV_{max}	5.5 ± 4.8	11.4 ± 7.2	7.4 ± 4.9	5.128	0.009#
FAPI SUV_{max}	7.2 ± 4.5	9.7 ± 3.0	7.5 ± 3.7	1.330	0.272
FDG SUV_{mean}	3.9 ± 3.1	8.0 ± 4.0	5.1 ± 3.3	6.437	0.003#
FAPI SUV_{mean}	5.0 ± 2.9	5.9 ± 1.9	5.0 ± 2.2	0.406	0.668
*: differences among groups caused by Inf & G. #: differences among groups caused by AC.					

Table 2

Diagnosis efficacy of NSCLC nodules in [^{68}Ga]Ga-DOTA-FAPI-04 and [^{18}F]FDG PET/CT

Diagnosis efficacy	FDG	FAPI
SEN	0.67	0.88
SPEC	0.13	0.13
ACC	0.60	0.79
PPV	0.85	0.88
NPV	0.05	0.14

SEN: sensitivity; SPEC: specificity; ACC: accuracy; PPV: positive predict value; NPV: negative predict value.

High uptake of [^{68}Ga]Ga-DOTA-FAPI-04 exhibited in AC, SCC and Inf & G nodule types, and the differences among them were not statistically significant. These three types showed high uptake of [^{18}F]FDG as well, in which SCC was higher than that of AC, but the difference between NSCLC and inflammation was not statistically significant. Meanwhile, there was no differences in blood pool uptake of [^{68}Ga]Ga-DOTA-FAPI-04 and [^{18}F]FDG (Fig. 2A). Diagnostic efficacy of [^{68}Ga]Ga-DOTA-FAPI-04 in NSCLC was better than [^{18}F]FDG PET/CT, as the diagnostic accuracy was 0.79 and 0.6 respectively in this study with criteria as $SUV_{max} \geq 2.5$ (**Table. 2**).

The AC nodules were further analyzed with respect to the densities. SN showed high uptake of both [^{68}Ga]Ga-DOTA-FAPI-04 and [^{18}F]FDG, while low uptake exhibited in GGN with no significant difference between two radiotracers. Though medium uptake exhibited in PSN, the uptake of [^{68}Ga]Ga-DOTA-FAPI-04 was higher than [^{18}F]FDG with significant differences (SUV_{max} were 4.8 ± 2.8 and 2.1 ± 1.1, $p = 0.003$) (Fig. 2B). A typical case where PSN of AC showed high uptake of [^{68}Ga]Ga-DOTA-FAPI-04 but with low uptake of [^{18}F]FDG is presented. The immunohistopathology (IHC) result verified high FAP expression in tumor interstitials (Fig. 3).

Diagnostic efficacy comparison of [^{68} Ga]Ga-DOTA-FAPI-04 and [^{18} F]FDG PET/CT in N staging of NSCLC patients

Totally, 100 LNs in 35 patients were enrolled, 17 of 35 (48.6%) patients companied with only non-metastatic LNs, while 18 of 35 (51.4%) patients have metastatic LNs. The diagnosis of non-metastatic LNs were obtained from post-surgery pathological results in 15 patients, and follow-up imaging confirmed such LNs in two patients. Eight patients with metastatic LNs were diagnosed by either resection or aspiration biopsy pathological results and ten patients were diagnosed by follow-up imaging. All these 100 LNs were assigned to metastatic (36 lesions) or non-metastatic (64 lesions) group depending on final diagnosis.

Imaging characteristics of LNs is shown in Table 3. The metastatic group tended to show lower density and larger short diameter, while no significant differences existed in risk categories and calcification between metastatic and non-metastatic groups. SUV of [^{68}Ga]Ga-DOTA-FAPI-04 was effective in differentiating metastatic and non-metastatic groups, with a higher uptake in the metastatic group, while SUV of [^{18}F]FDG did not show differences between the two groups. Moreover, SUV of [^{68}Ga]Ga-DOTA-FAPI-04 was lower than [^{18}F]FDG in the non-metastatic group ($p < 0.01$) and higher than [^{18}F]FDG in the metastatic group ($p < 0.01$) (Fig. 4). This indicated the potential of ^{68}Ga-DOTA-FAPI-04 for differential diagnosis of metastatic and non-metastatic LNs. One case (Fig. 5) depicted that several high uptake LNs which were suspected as metastatic LNs in [^{18}F]FDG showed low uptake of [^{68}Ga]Ga-DOTA-FAPI-04. The post-resection pathological result showed adenocarcinoma with no metastatic LNs (0 / 20),and the FAP expression was low as confirmed by IHC.

Table 3
Imaging characteristics of lymph nodes (by lesions)

Characteristics	Metastatic (%)	Non-metastatic (%)	χ^2 or t	p
Lesions	36	64		
Risk categories				
High	22 (61.1)	31 (48.4)		
Intermediate	6 (16.7)	10 (15.6)	2.112*	0.348
Low	8 (22.2)	23 (35.9)		
Density				
High	6 (16.7)	37 (57.8)		
Iso-density	22 (61.1)	27 (42.2)	24.977*	0.000
Low	8 (22.2)	0		
Calcification	2 (5.6)	9 (14.1)	1.703*	0.319
Short diameter (cm)	1.2 ± 0.54	0.8 ± 0.16	-5.314#	0.000
FDG SUV_{max}	6.5 ± 3.30	6.1 ± 2.32	-0.754#	0.453
FAPI SUV_{max}	10.7 ± 4.72	3.1 ± 1.29	-12.233#	0.000
FDG SUV_{mean}	4.9 ± 2.10	4.5 ± 1.46	-1.270#	0.207
FAPI SUV_{mean}	7.4 ± 3.13	2.5 ± 0.96	-11.576#	0.000
FAPI SUV_{max}/ FDG SUV_{max}	1.8 ± 0.93	0.5 ± 0.19	-10.975#	0.000

*, tested by chi-square test, χ^2 values were documented; #, t tested by Mann–Whitney U test, t values were documented.

Table 4
Multivariate logistic regression analysis of the relationship between PET parameters with metastatic LNs

Factor	Odds Ratio (95% CI)	p value
FAPI SUV_{max}	1.837 (1.189–2.838)	0.006
FAPI SUV_{max}/FDG SUV_{max}	11.438 (1.178-111.083)	0.036

Table 5
The diagnosis efficacy for identifying metastatic LNs

Criteria	By lesions			By cases		
	SEN(%)	SPEC(%)	ACC(%)	SEN(%)	SPEC(%)	ACC(%)
FDG SUV_{max}≥2.5	91.70	1.60	34	83.30	0	42.90
FAPI SUV_{max}≥6	86.10	100	95	77.80	100	88.60
Ratio#≥1.1	80.60	100	93	66.70	100	82.90
FAPI SUV_{max}≥6 or Ratio#≥1.1	89.20	100	97	83.30	100	91.40
#: Ratio: FAPI SUV_{max}/ FDG SUV_{max}; Sensitivity, SEN; Specificity, SPEC; Accuracy, ACC.						

Diagnostic efficacy of [^{68}Ga]Ga-DOTA-FAPI-04 was analyzed by taking parameters which could differentiate metastatic and non-metastatic groups into multivariate logistic regression, including density, short diameters, SUV_{max} of FAPI and FAPI SUV_{max}/ FDG SUV_{max}. The results indicated that FAPI SUV_{max} and FAPI SUV_{max}/FDG SUV_{max} could be used in differential diagnosis of metastatic and non-metastatic LNs while density and short diameters could not (**Table.4**). The area under receiver operating characteristic (ROC) curve of FAPI SUV_{max} and FAPI SUV_{max}/FDG SUV_{max} was 0.927 and 0.954, respectively (Fig. 6**)**, which indicated a prominent diagnostic ability of these two parameters.

FAPI SUV_{max} ≥6 and the ratio of FAPI SUV_{max}/FDG SUV_{max} ≥1.1 were set as the cut-off value to analyze the diagnostic efficacy by the perspective of lesions and cases. The combination of these two conditions and [^{18}F]FDG criteria were also analyzed and shown in **Table. 5**.

FAPI SUV_{max} and FAPI SUV_{max}/FDG SUV_{max} criteria identified more true negative cases than [^{18}F]FDG, however it made two more false negative cases than [^{18}F]FDG. Our result highlighted that LNs with low uptake of [^{68}Ga]Ga-DOTA-FAPI-04 and low FAPI SUV_{max}/FDG SUV_{max} were more likely to be non-metastatic LNs.

Diagnostic efficacy comparison of [^{68} Ga]Ga-DOTA-FAPI-04 and [^{18} F]FDG PET/CT in M staging of NSCLC patients

Nine patients with multi-metastatic lesions were enrolled in the study, and the lesion detectability of [^{68}Ga]Ga-DOTA-FAPI-04 PET/CT (206 lesions) was better than FDG PET/CT (106 lesions), but no patient's staging was changed. Tumor to blood-pool ratio (TBR) of [^{68}Ga]Ga-DOTA-FAPI-04 was higher than that of FDG with significant differences (6.5 ± 1.9 and 4.0 ± 2.0, $p < 0.05$). [^{68}Ga]Ga-DOTA-FAPI-04 PET/CT presented more abnormal uptake lesions than [^{18}F]FDG PET/CT in a multi-metastasis patient (Fig. 7).

Discussion

[^{68}Ga]Ga-DOTA-FAPI-04 is becoming a promising tracer for general tumor diagnosis with its low radiation dose, fast tracer kinetics, favorable tumor-to-background ratios and invulnerability towards blood glucose fluctuations[11]. Some clinical researches have revealed its applications in differential diagnosis and staging of several different kinds of tumors including glioblastomas, gastrointestinal tumors, hepatic nodules, etc.[12–15]. At present, pulmonary nodules stratifying and management mainly relies on the National Lung Screening Trial and Lung-RADS with CT imaging[24, 25], which indicated the probability of malignancy rather than diagnosis of NSCLC. Thus, diagnosis of NSCLC by any single examination remains a difficulty. The underlying advantages of [^{68}Ga]Ga-DOTA-FAPI-04 application in NSCLC have been discussed[12, 16], and studies indicated NSCLC with highly uptake of [^{68}Ga]Ga-DOTA-FAPI-04. Meanwhile, one case report concerning NSCLC revealed the appropriate imaging result of [^{68}Ga]Ga-DOTA-FAPI-04[26]. Here, the application of [^{68}Ga]Ga-DOTA-FAPI-04 in suspected or diagnosed NSCLC patients was evaluated in detail and compared with that of [^{18}F]FDG through a systematic study.

Morphological signs acquired on CT showed poor differential ability for NSCLC characterization of lung nodules, with the only statistically significant single indicator being the lobular sign. [^{18}F]FDG PET/CT has been demonstrated as a useful, yet incomplete, tool for lung nodules diagnosis. One of the main limitations is that many benign lesions also present high FDG uptake which can easily lead to false-positive results[27, 28]. SCC and solid nodules of AC showed high uptake of both [^{18}F]FDG and [^{68}Ga]Ga-DOTA-FAPI-04 because the solid components consist of densely packed tumor cells and peri-tumoral stroma, while GGO showed low uptake for lacking tumor cells and peri-tumoral stroma. Additionally, [^{68}Ga]Ga-DOTA-FAPI-04, similar to [^{18}F]FDG, could not differentiate inflammation nodules from NSCLC, which might be attributed to the inclusion criteria as clinical suspected or diagnosed NSCLC patients. Inflammatory nodules presenting high uptake of [^{68}Ga]Ga-DOTA-FAPI-04 might be due to the abundant activated fibroblast in inflammatory tissues[29]. Therefore, the false-positive cases caused by inflammation might be a relevant limitation for both [^{68}Ga]Ga-DOTA-FAPI-04 and [^{18}F]FDG. However, [^{68}Ga]Ga-DOTA-FAPI-04 has better performance than [^{18}F]FDG in NSCLC detection sensitivity (0.88 vs. 0.67).

It was reported that among incidentally-detected small pulmonary nodules, PSNs had a high malignant potential (62.5–89.6%)[30, 31]. In the case of adenocarcinoma appearing as SN, the SUV_{max} of [^{18}F]FDG has been reported to be relatively low, ranging from 0.4 to 2.6 (mean SUV_{max} 1.3)[32]. This phenomenon was also found in the present study, the mean [^{18}F]FDG SUV_{max} of PSNs of AC in our study was 2.1 ± 1.1. And the uptake of [^{68}Ga]Ga-DOTA-FAPI-04 (SUV_{max}: 4.8 ± 2.8) was higher than [^{18}F]FDG with significant differences, which might be attributed to that partial solid nodules of AC were relatively slow-growing cancers which do not actively use glucose but the interstitial component proliferate rapidly as IHC implied in Fig. 3[27].

N staging is crucial to the management and prognosis of NSCLC patients. However, previous studies have shown that metastatic LNs concerning NSCLC staging diagnosis remains difficult in [^{18}F]FDG PET/CT examination because high uptake of [^{18}F]FDG can be seen in reactive LNs in mediastinum and bilateral hilum, especially in hyperplasia, inflammation, infection and granulomatous disease[33, 34].The recognized consensus indicated that positive mediastinal nodal on PET/CT should be verified histologically by endobronchial ultrasound mediastinoscopy[35]. In our study, [^{18}F]FDG showed a satisfactory sensitivity albeit a poor specificity which was similar to the former studies[34]. Still, [^{68}Ga]Ga-DOTA-FAPI-04 showed excellent capacity to differentiate metastatic and non-metastatic LNs in multivariate regression analysis while other characteristics including density, calcification and short diameter all failed, as non-metastatic LNs exhibited much lower uptake than metastatic LNs. Therefore, [^{68}Ga]Ga-DOTA-FAPI-04 PET/CT is more specific than [^{18}F]FDG for identifying non-metastatic LNs not only by lesions but also by cases. [^{68}Ga]Ga-DOTA-FAPI-04 decreased the false positive rate sharply, which may boost the acceptance of non-invasive examinations in clinical decision-making. The ratio of SUV_{max} [^{68}Ga]Ga-DOTA-FAPI-04 to [^{18}F]FDG lower than 1.1 represented tendency to be non-metastatic LNs regardless of FAPI uptake level. The combination of [^{68}Ga]Ga-DOTA-FAPI-04 SUV_{max} and the ratio of the two tracers became a more accurate staging criteria of LNs than using [^{68}Ga]Ga-DOTA-FAPI-04 SUV_{max} alone. However, two more false negative cases existed from [^{68}Ga]Ga-DOTA-FAPI-04 than [^{18}F]FDG, and this might be attributed to the low FAP expression in small metastases which has been reported before[36]. Hence, the low FAPI uptake and low ratio of FAPI to FDG could attribute to the differential diagnosis of metastatic and non-metastatic LNs, these criteria help to identify more true negative patients who may avoid the invasive biopsy in clinical practice. This still requires further verification with more cases.

For M staging in this study, the average [^{18}F]FDG SUV_{max} of primary lesions was 12.4 ± 7.6. In 6 of the 9 patients, the primary lesion's 2-^{18}F-FDG SUV_{max} was 7.8 ± 2.2, which corresponded to a low to moderate [^{18}F]FDG uptake level of NSCLCs. [^{68}Ga]Ga-DOTA-FAPI-04 PET/CT revealed more high uptake lesions than [^{18}F]FDG in these patients, which indicated that [^{68}Ga]Ga-DOTA-FAPI-04 exhibited prominent supplementary function in multi-metastatic NSCLC patients with low [^{18}F]FDG uptake of lesions. Especially for those patients with metastasis in brain, skull and liver, [^{68}Ga]Ga-DOTA-FAPI-04 images showed lower background activity and higher image contrast than [^{18}F]FDG [37]. As in the case depicted (**Figure. 7**), small metastasis of skull is easily missed on [^{18}F]FDG images, due to the high uptake level of brain, but it was exhibited apparently in [^{68}Ga]Ga-DOTA-FAPI-04 PET/CT, which is consistent with former studies[16].

As a first systemic research trying to evaluate the role of [^{68}Ga]Ga-DOTA-FAPI-04 PET/CT in NSCLC patients, there are several limitations of this study. First, the number of patients was relatively limited, with the inclusion criteria as clinical suspected or diagnosed NSCLC patients most lung nodules turned out to be adenocarcinoma, thus a small amount (8 patients) of inflammation patients enrolled, which

restricted the analysis between NSCLC and inflammation. Moreover, there was an imbalance between the number of metastatic (36 lesions) and non-metastatic (64 lesions) LNs, which restricted the convincingness of better diagnostic specificity in [^{68}Ga]Ga-DOTA-FAPI-04 PET/CT in some way. A larger number of LNs in further study, especially metastatic LNs, along with part of LNs performed for criteria verification would strengthen present conclusions. Although [^{68}Ga]Ga-DOTA-FAPI-04 possessed a better detectability in multi-metastatic patients with lower background uptake than [^{18}F]FDG, it showed no changes to the patient's treatment strategy, which might be attributed to the small number of multi-meta patients (9 cases). We hope future clinical studies and systematic reviews may help to better understand the impact of [^{68}Ga]Ga-DOTA-FAPI-04 PET/CT scans on the treatment strategy of NSCLC patients.

Conclusion

The results showed that [^{68}Ga]Ga-DOTA-FAPI-04 PET/CT was able to detect primary NSCLC lesions with higher sensitivity than [^{18}F]FDG. At the same time, [^{68}Ga]Ga-DOTA-FAPI-04 PET/CT increased specificity of detecting metastatic LNs and detection of multi-metastatic lesions. The potential value of [^{68}Ga]Ga-DOTA-FAPI-04 PET/CT was exhibited which indicated its regular application in NSCLC diagnosis and staging was feasible.

Declarations

Funding: The current research was financially supported by the National Natural Science Foundation of China 81671733, 81871386, and 81871387, Natural Science Foundation of Beijing project 7202027, and Science Foundation of Peking University Cancer Hospital-2021-18.

Consent of interests: The authors have declared that no competing interests exist.

Availability of data and material: All data relevant to the study are included in the article or uploaded as supplementary information.

Code availability: Not applicable.

Ethics approval and consent to participate: This study was approved by the Medical Ethics Committee of Peking University Cancer Hospital (2019 KT95), oral and written informed consent was obtained from all participants.

Consent for publication: Not required.

References

1. Kalluri R. The biology and function of fibroblasts in cancer. Nature Reviews Cancer. 2016;16:582-98. doi:10.1038/nrc.2016.73.

2. Santi A, Kugeratski FG, Zanivan S. Cancer Associated Fibroblasts: The Architects of Stroma Remodeling. Proteomics. 2018;18. doi:10.1002/pmic.201700167.
3. Liao Z, Tan ZW, Zhu P, Tan NS. Cancer-associated fibroblasts in tumor microenvironment - Accomplices in tumor malignancy. Cell Immunol. 2019;343:103729. doi:10.1016/j.cellimm.2017.12.003.
4. McCarthy JB, El-Ashry D, Turley EA. Hyaluronan, Cancer-Associated Fibroblasts and the Tumor Microenvironment in Malignant Progression. Front Cell Dev Biol. 2018;6:48. doi:10.3389/fcell.2018.00048.
5. Han Y, Zhang Y, Jia T, Sun Y. Molecular mechanism underlying the tumor-promoting functions of carcinoma-associated fibroblasts. Tumour Biol. 2015;36:1385-94. doi:10.1007/s13277-015-3230-8.
6. Koczorowska MM, Tholen S, Bucher F, Lutz L, Kizhakkedathu JN, De Wever O, et al. Fibroblast activation protein-alpha, a stromal cell surface protease, shapes key features of cancer associated fibroblasts through proteome and degradome alterations. Mol Oncol. 2016;10:40-58. doi:10.1016/j.molonc.2015.08.001.
7. Garin-Chesa P, Old LJ, Rettig WJ. Cell surface glycoprotein of reactive stromal fibroblasts as a potential antibody target in human epithelial cancers. Proceedings of the National Academy of Sciences of the United States of America. 1990;87:7235-9. doi:10.1073/pnas.87.18.7235.
8. Lai D, Ma L, Wang F. Fibroblast activation protein regulates tumor-associated fibroblasts and epithelial ovarian cancer cells. Int J Oncol. 2012;41:541-50. doi:10.3892/ijo.2012.1475.
9. Loktev A, Lindner T, Mier W, Debus J, Altmann A, Jager D, et al. A Tumor-Imaging Method Targeting Cancer-Associated Fibroblasts. J Nucl Med. 2018;59:1423-9. doi:10.2967/jnumed.118.210435.
10. Lindner T, Loktev A, Altmann A, Giesel F, Kratochwil C, Debus J, et al. Development of Quinoline-Based Theranostic Ligands for the Targeting of Fibroblast Activation Protein. J Nucl Med. 2018;59:1415-22. doi:10.2967/jnumed.118.210443.
11. Giesel FL, Kratochwil C, Lindner T, Marschalek MM, Loktev A, Lehnert W, et al. (68)Ga-FAPI PET/CT: Biodistribution and Preliminary Dosimetry Estimate of 2 DOTA-Containing FAP-Targeting Agents in Patients with Various Cancers. J Nucl Med. 2019;60:386-92. doi:10.2967/jnumed.118.215913.
12. Kratochwil C, Flechsig P, Lindner T, Abderrahim L, Altmann A, Mier W, et al. (68)Ga-FAPI PET/CT: Tracer Uptake in 28 Different Kinds of Cancer. J Nucl Med. 2019;60:801-5. doi:10.2967/jnumed.119.227967.
13. Rohrich M, Loktev A, Wefers AK, Altmann A, Paech D, Adeberg S, et al. IDH-wildtype glioblastomas and grade III/IV IDH-mutant gliomas show elevated tracer uptake in fibroblast activation protein-specific PET/CT. Eur J Nucl Med Mol Imaging. 2019;46:2569-80. doi:10.1007/s00259-019-04444-y.
14. Koerber SA, Staudinger F, Kratochwil C, Adeberg S, Haefner MF, Ungerechts G, et al. The Role of (68)Ga-FAPI PET/CT for Patients with Malignancies of the Lower Gastrointestinal Tract: First Clinical Experience. J Nucl Med. 2020;61:1331-6. doi:10.2967/jnumed.119.237016.
15. Shi X, Xing H, Yang X, Li F, Yao S, Zhang H, et al. Fibroblast imaging of hepatic carcinoma with (68)Ga-FAPI-04 PET/CT: a pilot study in patients with suspected hepatic nodules. Eur J Nucl Med

Mol Imaging. 2020. doi:10.1007/s00259-020-04882-z.

16. Chen H, Pang Y, Wu J, Zhao L, Hao B, Wu J, et al. Comparison of [(68)Ga]Ga-DOTA-FAPI-04 and [(18)F] FDG PET/CT for the diagnosis of primary and metastatic lesions in patients with various types of cancer. Eur J Nucl Med Mol Imaging. 2020;47:1820-32. doi:10.1007/s00259-020-04769-z.
17. Zhao YR, Heuvelmans MA, Dorrius MD, van Ooijen PM, Wang Y, de Bock GH, et al. Features of resolving and nonresolving indeterminate pulmonary nodules at follow-up CT: the NELSON study. Radiology. 2014;270:872-9. doi:10.1148/radiol.13130332.
18. Eisenhauer EA, Therasse P, Bogaerts J, Schwartz LH, Sargent D, Ford R, et al. New response evaluation criteria in solid tumours: revised RECIST guideline (version 1.1). Eur J Cancer. 2009;45:228-47. doi:10.1016/j.ejca.2008.10.026.
19. Kakinuma R, Noguchi M, Ashizawa K, Kuriyama K, Maeshima AM, Koizumi N, et al. Natural History of Pulmonary Subsolid Nodules: A Prospective Multicenter Study. Journal of thoracic oncology : official publication of the International Association for the Study of Lung Cancer. 2016;11:1012-28. doi:10.1016/j.jtho.2016.04.006.
20. Gould MK, Maclean CC, Kuschner WG, Rydzak CE, Owens DK. Accuracy of positron emission tomography for diagnosis of pulmonary nodules and mass lesions: a meta-analysis. Jama. 2001;285:914-24. doi:10.1001/jama.285.7.914.
21. Lowe VJ, Fletcher JW, Gobar L, Lawson M, Kirchner P, Valk P, et al. Prospective investigation of positron emission tomography in lung nodules. Journal of clinical oncology : official journal of the American Society of Clinical Oncology. 1998;16:1075-84. doi:10.1200/jco.1998.16.3.1075.
22. Mattes MD, Weber WA, Foster A, Moshchinsky AB, Ahsanuddin S, Zhang Z, et al. A Predictive Model for Lymph Node Involvement with Malignancy on PET/CT in Non–Small-Cell Lung Cancer. Journal of Thoracic Oncology. 2015;10:1207-12. doi:10.1097/jto.0000000000000601.
23. Hellwig D, Graeter TP, Ukena D, Groeschel A, Sybrecht GW, Schaefers HJ, et al. 18F-FDG PET for mediastinal staging of lung cancer: which SUV threshold makes sense? J Nucl Med. 2007;48:1761-6. doi:10.2967/jnumed.107.044362.
24. Aberle DR, Adams AM, Berg CD, Black WC, Clapp JD, Fagerstrom RM, et al. Reduced lung-cancer mortality with low-dose computed tomographic screening. The New England journal of medicine. 2011;365:395-409. doi:10.1056/NEJMoa1102873.
25. American College of Radiology (2014) Lung-RADS™ Version 1.0 Assessment Categories.
26. Giesel FL, Heussel CP, Lindner T, Röhrich M, Rathke H, Kauczor H-U, et al. FAPI-PET/CT improves staging in a lung cancer patient with cerebral metastasis. European Journal of Nuclear Medicine and Molecular Imaging. 2019;46:1754-5. doi:10.1007/s00259-019-04346-z.
27. Maiga AW, Deppen SA, Mercaldo SF, Blume JD, Montgomery C, Vaszar LT, et al. Assessment of Fluorodeoxyglucose F18-Labeled Positron Emission Tomography for Diagnosis of High-Risk Lung Nodules. JAMA Surg. 2018;153:329-34. doi:10.1001/jamasurg.2017.4495.
28. Chen S, Harmon S, Perk T, Li X, Chen M, Li Y, et al. Diagnostic classification of solitary pulmonary nodules using dual time (18)F-FDG PET/CT image texture features in granuloma-endemic regions.

Sci Rep. 2017;7:9370. doi:10.1038/s41598-017-08764-7.

29. Luo Y, Pan Q, Yang H, Peng L, Zhang W, Li F. Fibroblast activation protein targeted PET/CT with (68)Ga-FAPI for imaging IgG4-related disease: comparison to (18)F-FDG PET/CT. J Nucl Med. 2020. doi:10.2967/jnumed.120.244723.
30. Nakata M, Saeki H, Takata I, Segawa Y, Mogami H, Mandai K, et al. Focal ground-glass opacity detected by low-dose helical CT. Chest. 2002;121:1464-7. doi:10.1378/chest.121.5.1464.
31. Henschke CI, Yankelevitz DF, Mirtcheva R, McGuinness G, McCauley D, Miettinen OS. CT screening for lung cancer: frequency and significance of part-solid and nonsolid nodules. AJR American journal of roentgenology. 2002;178:1053-7. doi:10.2214/ajr.178.5.1781053.
32. Chun EJ, Lee HJ, Kang WJ, Kim KG, Goo JM, Park CM, et al. Differentiation between malignancy and inflammation in pulmonary ground-glass nodules: The feasibility of integrated (18)F-FDG PET/CT. Lung Cancer. 2009;65:180-6. doi:10.1016/j.lungcan.2008.11.015.
33. Konishi J, Yamazaki K, Tsukamoto E, Tamaki N, Onodera Y, Otake T, et al. Mediastinal lymph node staging by FDG-PET in patients with non-small cell lung cancer: analysis of false-positive FDG-PET findings. Respiration. 2003;70:500-6. doi:10.1159/000074207.
34. Al-Sarraf N, Gately K, Lucey J, Wilson L, McGovern E, Young V. Lymph node staging by means of positron emission tomography is less accurate in non-small cell lung cancer patients with enlarged lymph nodes: analysis of 1,145 lymph nodes. Lung Cancer. 2008;60:62-8. doi:10.1016/j.lungcan.2007.08.036.
35. De Leyn P, Lardinois D, Van Schil P, Rami-Porta R, Passlick B, Zielinski M, et al. European trends in preoperative and intraoperative nodal staging: ESTS guidelines. Journal of thoracic oncology : official publication of the International Association for the Study of Lung Cancer. 2007;2:357-61. doi:10.1097/01.JTO.0000263722.22686.1c.
36. Serfling S, Zhi Y, Schirbel A, Lindner T, Meyer T, Gerhard-Hartmann E, et al. Improved cancer detection in Waldeyer's tonsillar ring by 68Ga-FAPI PET/CT imaging. European Journal of Nuclear Medicine and Molecular Imaging. 2020. doi:10.1007/s00259-020-05055-8.
37. Sivesgaard K, Larsen LP, Sorensen M, Kramer S, Schlander S, Amanavicius N, et al. Diagnostic accuracy of CE-CT, MRI and FDG PET/CT for detecting colorectal cancer liver metastases in patients considered eligible for hepatic resection and/or local ablation. Eur Radiol. 2018;28:4735-47. doi:10.1007/s00330-018-5469-0.

Figures

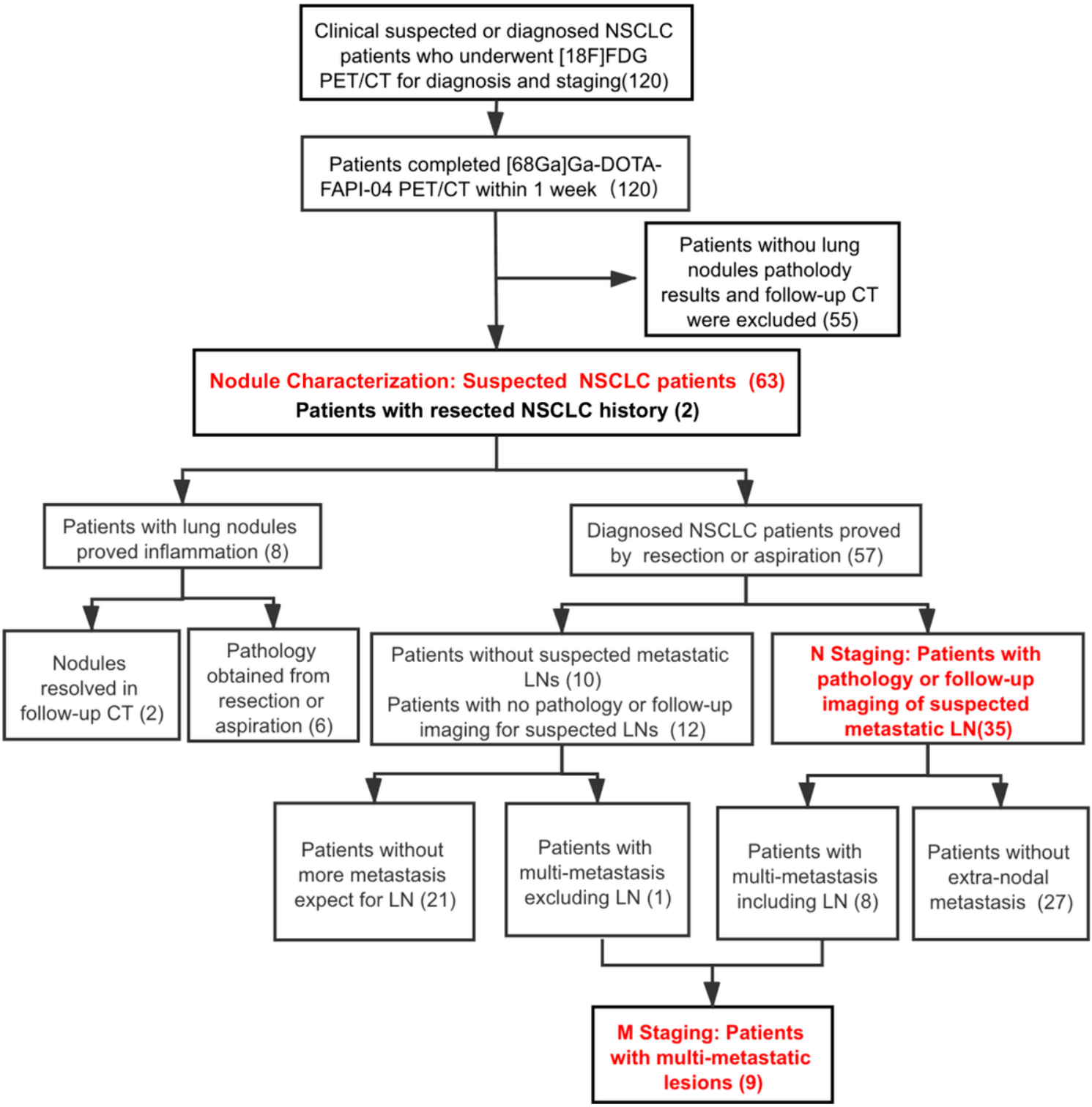

Figure 1

Inclusion, exclusion criteria and grouping

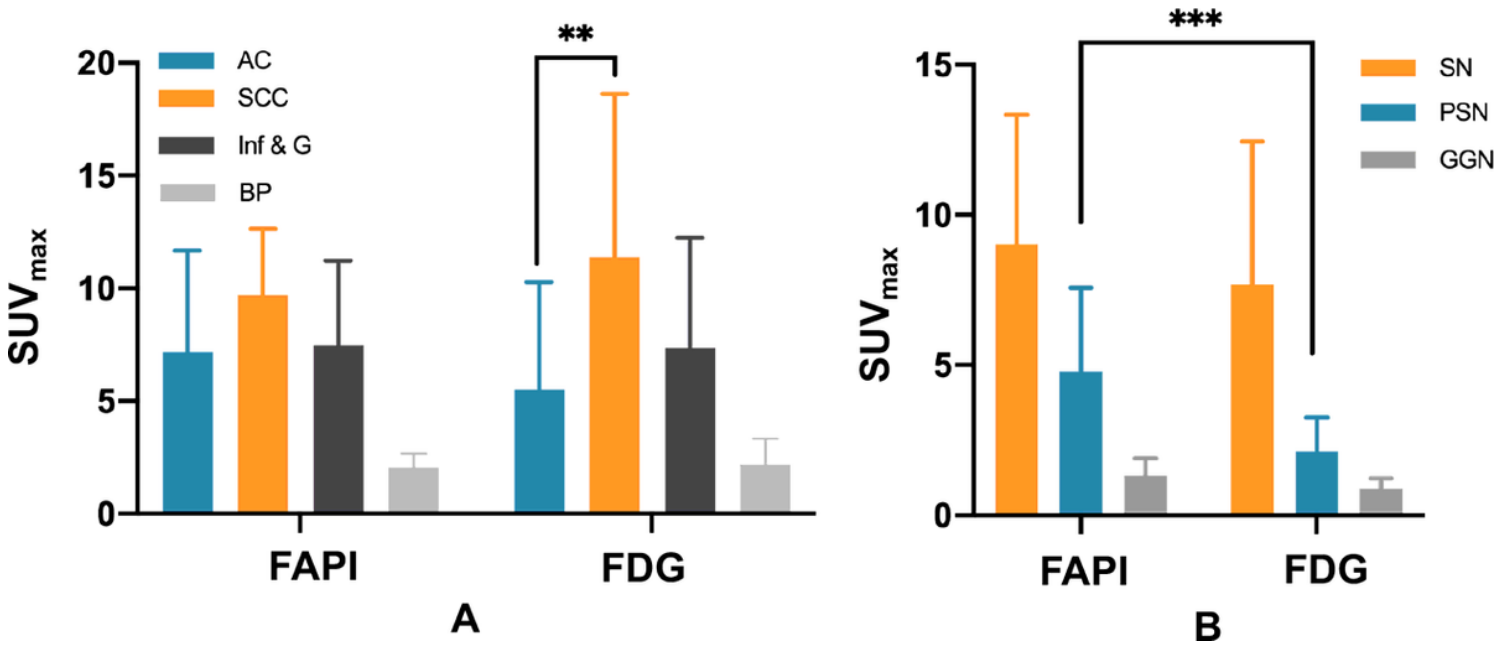

Figure 2

The uptake values of 68Ga-DOTA-FAPI-04 and 2-18F-FDG for adenocarcinoma (AC), squamous cell carcinoma (SCC), inflammation & granuloma (Inf & G) and blood pool (BP). The uptake of [68Ga]Ga-DOTA-FAPI-04 and [18F]FDG for three composition nodules as solid nodules (SN), partial solid nodules (PSN) and ground glass nodules (GGN) of AC (B). *, significant differences.

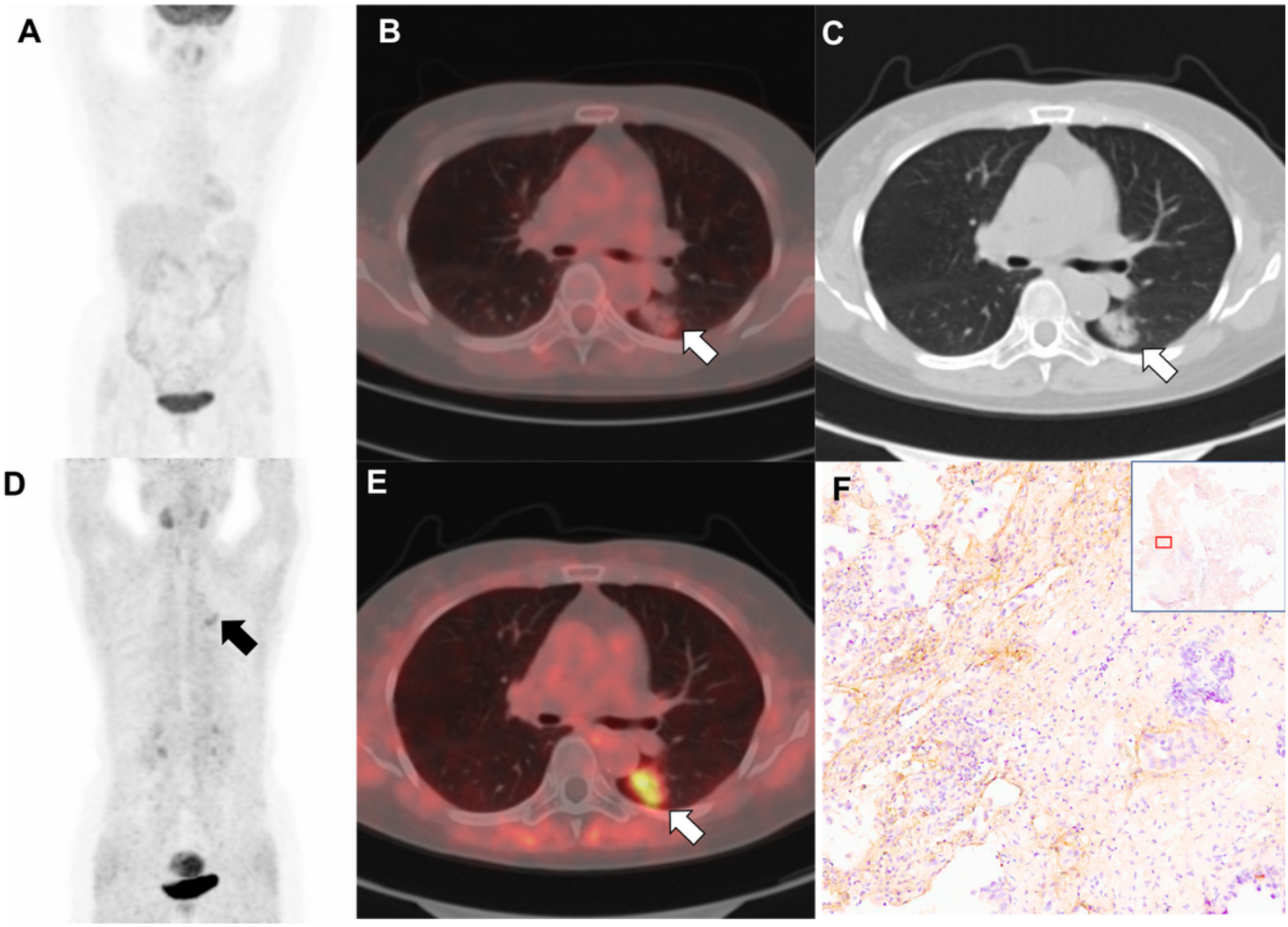

Figure 3

A sixty-year-old female with partial solid nodule in the lower lobe of left lung proved as adenocarcinoma. SUVmax of the lung nodule on [18F]FDG PET/CT was 1.6 (A, MIP (maximal intensity projection), B, axial PET/CT fusion, C, axial CT); SUVmax of the lung nodule on [68Ga]Ga-DOTA-FAPI-04 PET/CT was 5.2 (D, E). Immunohistopathology result proved high FAP expression in tumor interstitials (F).

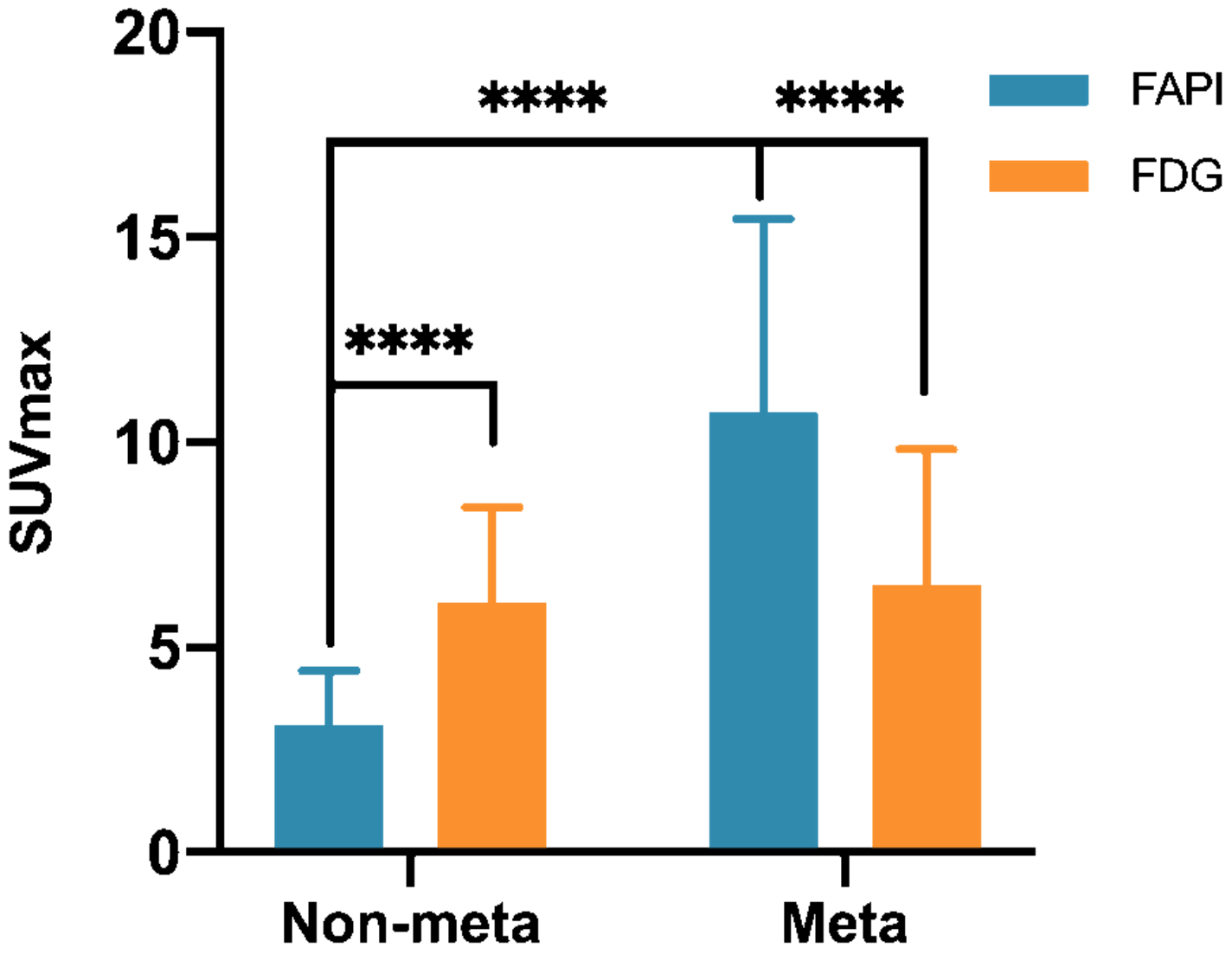

Figure 4

The uptake of [68Ga]Ga-DOTA-FAPI-04 and [18F]FDG in metastatic (meta) and non-metastatic (non-meta) LNs. *, significant differences.

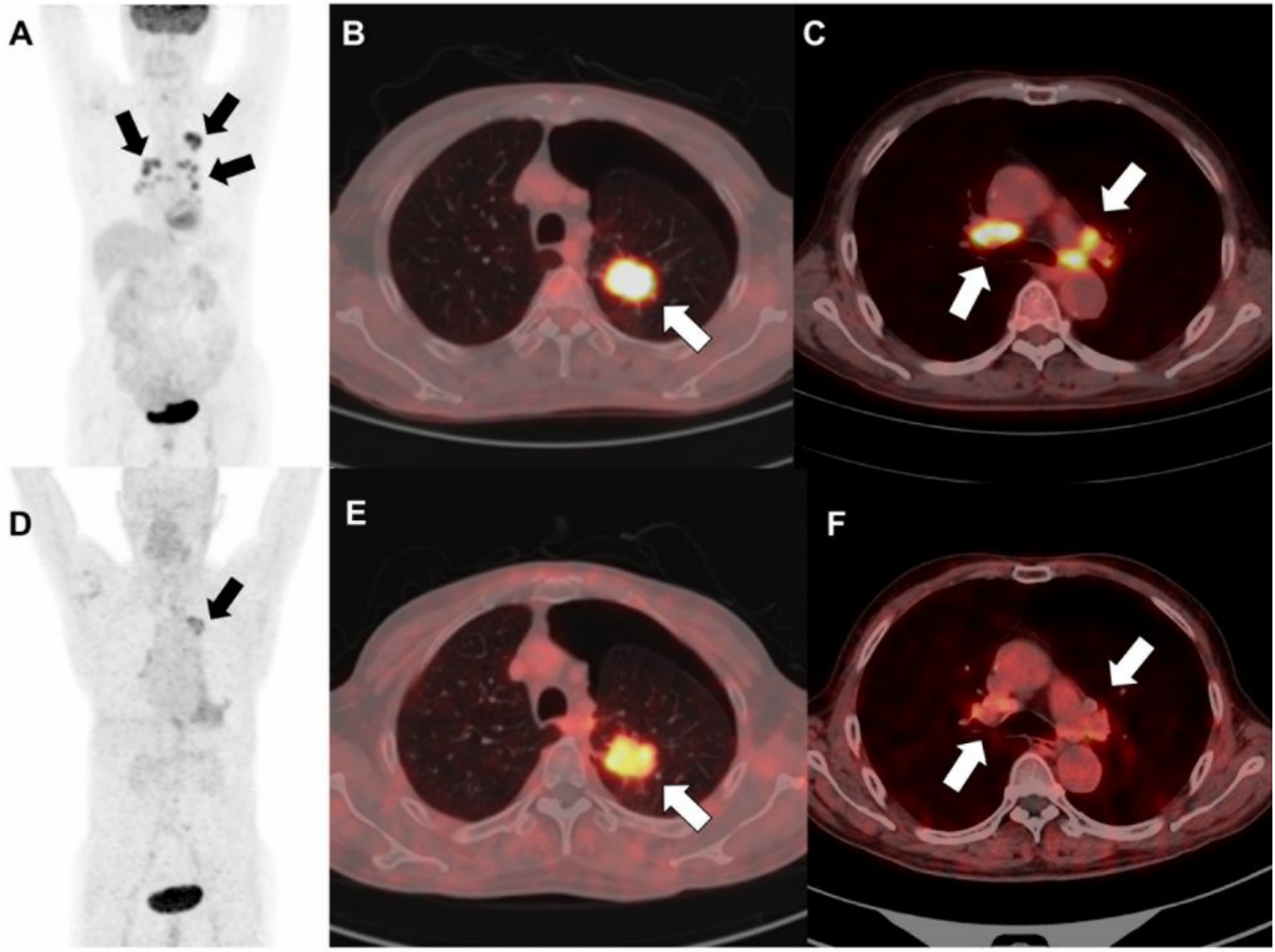

Figure 5

A seventy-seven-year-old man proved as squamous cell carcinoma in the upper lobe of left lung with non-metastatic LNs. SUVmax of lung nodule and LNs in [18F]FDG PET/CT was 11 and 8.2, respectively (A, B, C); SUVmax of lung nodule and LNs in [68Ga]Ga-DOTA-FAPI-04 PET/CT was 6.4 and 3 (D, E, F).

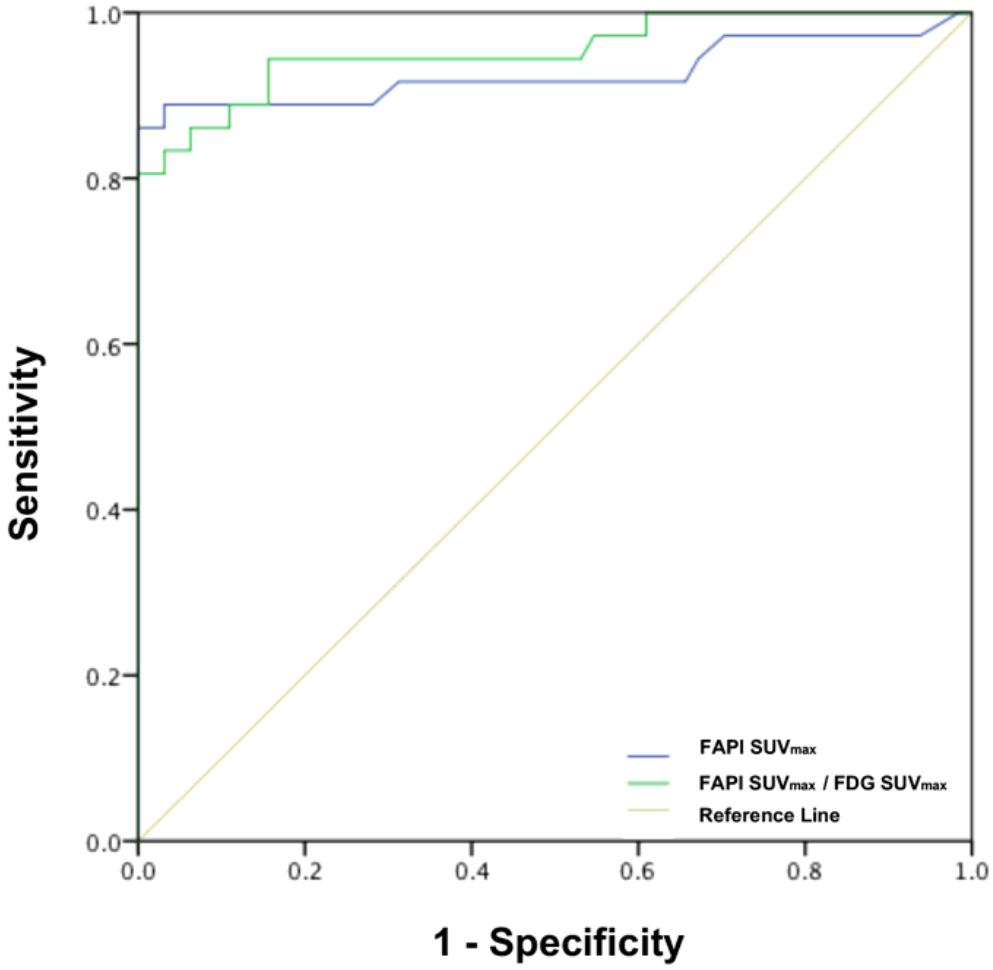

Figure 6

ROC curve for parameters in identifying metastatic LNs.

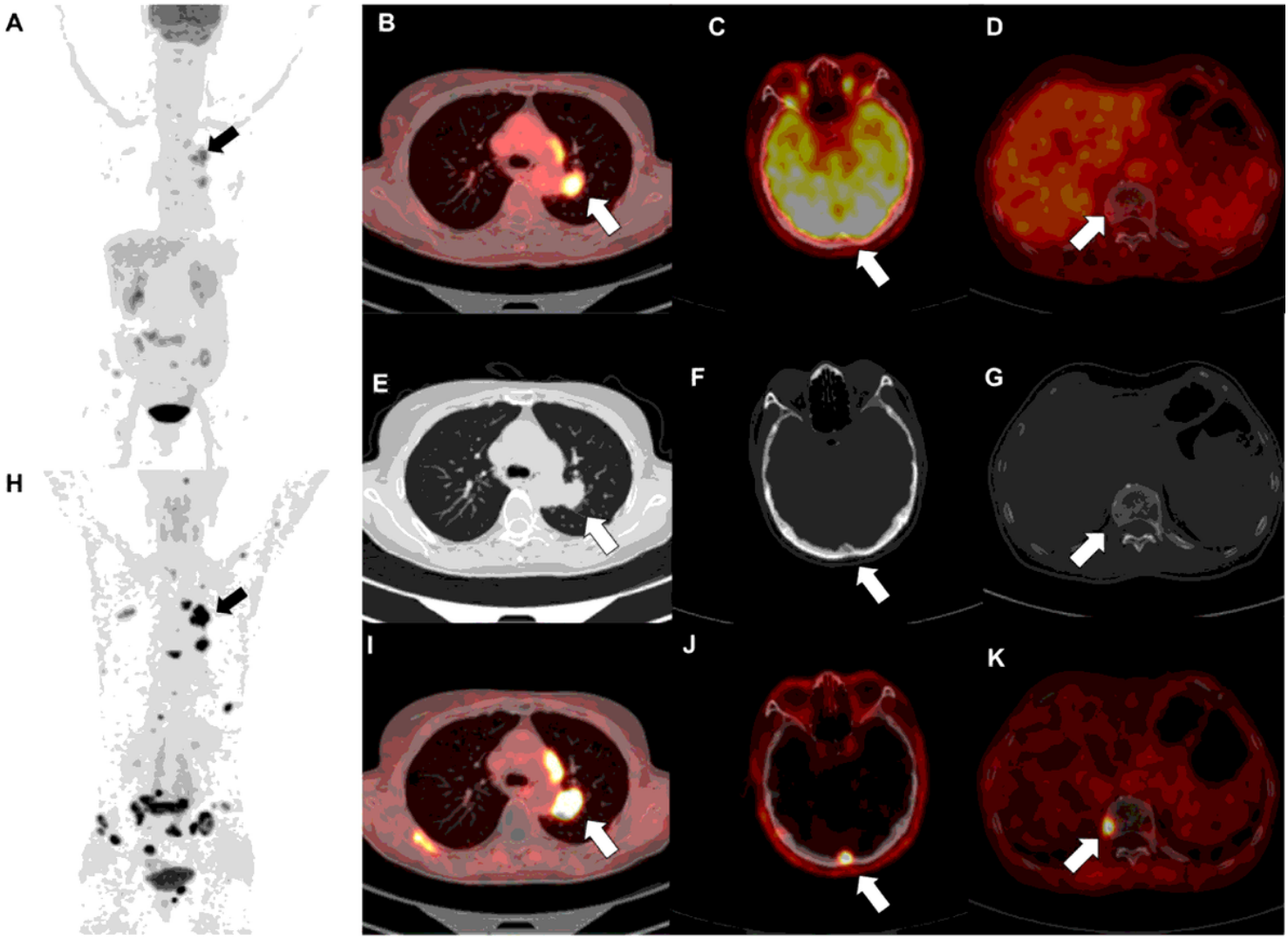

Figure 7

A sixty-seven-year-old woman with adenocarcinoma in the upper lobe of left lung. SUVmax of the lung nodule and vertebral metastases in [18F]FDG PET/CT was 7.8 and 2.7 respectively (A, B, D). Lesions adjacent to skull were not clearly observed in FDG imaging, and the precise SUV value could not be obtained due to the influence of high brain uptake (C); E, F, G show axial CT images of lesions. SUVmax of the lung nodule, skull and vertebral metastases in [68Ga]Ga-DOTA-FAPI-04 PET/CT was 18.9, 8.2 and 9.4, respectively (H, I, J, K).

Supplementary Files

This is a list of supplementary files associated with this preprint. Click to download.

- supplementaryinformation.docx